J. Eur. Opt. Society-Rapid Publ. 2024, **20**, 15
© The Author(s), published by EDP Sciences, 2024
https://doi.org/10.1051/jeos/2024015
Available online at: https://jeos.edpsciences.org

Special Issue - Plasmonica 2023
Antonino Foti and Attilio Zilli (Guest editors)

Journal of the European Optical Society-Rapid Publications

RESEARCH ARTICLE OPEN ACCESS

Polarization-resolved surface-enhanced infrared spectra with nanosensors based on self-organized gold nanorods

Raffaella Polito[1,*], S. Sotgiu[1], F. Sohrabi[2], G. Ferrando[3], F. Berkmann[1], M. E. Temperini[1,2], V. Giliberti[2], F. Buatier de Mongeot[3], M. Ortolani[1], L. Baldassarre[1], and M.C. Giordano[3]

[1] Department of Physics, Sapienza University of Rome, P.le A. Moro 2, I-00185 Rome, Italy
[2] Center for Life Nano-Science, Istituto Italiano di Tecnologia, Viale Regina Elena 291, I-00161 Rome, Italy
[3] Dipartimento di Fisica, Università degli Studi di Genova, Via Dodecaneso 33, I-16146 Genova, Italy

Received 31 January 2024 / Accepted 28 March 2024

Abstract. Biosensors are becoming ubiquitous in the study of biomolecules, as, by modifying shape size and environment of metallic nanostructures it is now possible to engineer the field so to monitor subtle transient changes in molecular conformation at the level of a single biolayer. In this paper, we present a first step towards a polarization-resolved study of light-induced conformational changes of transmembrane proteins. We exploit a platform of self-organized gold nanorods on SiO_2 substrates to enhance the infrared reflection absorption spectroscopy and to perform difference spectroscopy (*i.e.*, spectrum under visible light ON minus spectrum under visible light OFF) on a light-sensitive transmembrane protein with simultaneous visible light illumination from the backside of the chip. The broad size distribution of nanorods allows us to probe with high sensitivity the modifications of the vibrational peaks over the entire fingerprint region. We show that it is possible to identify dissimilarities in the difference spectra, which in turn implies that we are monitoring over a broadband spectrum not only the chemical bonds with the dipole moment aligned orthogonally to our substrate/nanorod surface but also those with different orientation.

Keywords: Self-organized nanoantennas, IR sensing, IRRAS, Near-field IR nanospectroscopy.

1 Introduction

Biosensors for the detection and the study of thin biolayers hold great promise for applications in biotechnology, medical research, clinical diagnostics, and pharmaceutical sciences [1–4]. A great scientific and technological challenge is to design a biosensor capable of monitoring real-time functional modifications of an extremely low number of proteins triggered by external perturbations that could allow a deep understanding of protein conformational changes underlaying the biological functional reaction steps [5, 6].

Of particular interest is the study of transmembrane proteins, *i.e.*, proteins spanning across the cell membrane that are often targeted for drug delivery [7].

With its high accuracy in monitoring frequency-dependent modification in chemical bonds, mid-Infrared (mid-IR) spectroscopy (2–20 μm in wavelength) is the technique of choice for characterizing transient protein conformational changes [8, 9]. The poor sensitivity of mid-IR spectroscopy however can be a limiting factor for its use to study a single biolayer. Several approaches have been developed to overcome the limit of sensitivity, such as Infrared Reflection Absorption Spectroscopy (IRRAS) that is a well-established tool for measuring thin biolayers deposited on metal substrates, thanks to its high surface sensitivity [10, 11]. However, at grazing incident angle of IR radiation only the Transverse Magnetic (TM) modes of the Electric field (E) are sustained by a continuous metal surface due to the surface selection rule [12]. Therefore, only the protein dipole moments parallel to the surface normal can be excited, while information about the perpendicular ones is prevented. In order to monitor conformational changes and orientation of protein thin layers with both polarizations (TM and Transverse Electric (TE)), one has to resort to different strategies such as the use of Bloch Surface Waves [13] and/or of plasmonic nanoantennas. Notably, nanoantennas can be designed to excite plasmonic resonances with both TM- and TE-polarized light by changing the relative orientation of the nanoantennas with the E [14, 15].

Usually, in order to achieve a high sensitivity, nanoantennas are designed with high quality factors [16–19], leading to sharp resonances. Therefore, the overlap of the antenna modes with the resonant vibrational modes of

* Corresponding author: raffaella.polito@uniroma1.it

This is an Open Access article distributed under the terms of the Creative Commons Attribution License (https://creativecommons.org/licenses/by/4.0), which permits unrestricted use, distribution, and reproduction in any medium, provided the original work is properly cited.

interest can only occur on a small frequency range and not in the entire "fingerprint region" (2–20 μm, 500–5000 cm^{-1}) that should instead be investigated, to monitor the complex functional mechanism of proteins. One possibility to overcome this obstacle is to design and perform subsequent experiments with several platforms of nanorods of different size with shortcomings in terms of both fabrication difficulties as well as sample and time consumption [20–23].

Here we propose a novel large-area platform for perspective polarization-resolved biosensor based on randomly sized self-organized gold nanorods deposited on nanopatterned glass templates and measured in reflection at grazing angles for the study of light-induced conformational changes of transmembrane proteins. We characterize the broad distribution of hotspots within a large sample area with IR nanospectroscopy and we perform a proof of principle experiment on Bacteriorhodopsin (BR) [24, 25]. With this easy-to-use platform, one can illuminate from the backside with visible radiation to induce the protein conformational change while monitoring the IR spectrum over the entire fingerprint region with high sensitivity, in principle down to the single biolayer.

In particular, we show that with our nanorod platform we find two distinct difference absorption spectra for incoming TM- or TE-polarized light, enabling polarization-resolved IRRAS spectroscopy over a broadband frequency range on biomolecules at variance with the current approaches in literature.

2 Results and discussion

2.1 Morphological and far-field optical characterization of nanorod array platforms

Based on a previously developed design for surface enhanced spectroscopies [26–28], we designed and produced a plasmonic platform for Surface-Enhanced Infrared Absorption Spectroscopy (SEIRA) consisting of anisotropic arrays of randomly sized gold nanorods deposited on rippled glass templates [29–31] by glancing angle thermal deposition at 70°. Figures 1a and 1c present a visible image of the sample that is homogeneous over large area (cm^2 scale), and the sketch of its ripple cross section. Morphological characterization of these self-organized arrays was performed by means of Scanning Electron Microscopy (SEM, Fig. 1b) and Atomic Force Microscopy (AFM, Fig. 1d), confirming the anisotropic ordering of the arrays along the axis defined as x, and the random distribution of the nanorods length between hundreds of nanometres and 3–4 μm. The profile analysis of the AFM topography images shows a Root Mean Square (RMS) roughness of 24 nm and a pattern periodicity (lateral distance between two nanorods) of 174 nm.

The nanorod platform is designed to perform an IRRAS experiment while exciting the sample deposited on it from the backside with visible light. We have thus characterized the transmission of the platform in far-field in both the visible (VIS) and IR regions (see Fig. 1e for a sketch of the optical setup) of the spectra. The data in Figures 1f and 1g show transmittance values above 0.8 when E is polarized perpendicular to the long nanorod axis. Transmittance settles to values above 0.6 for the other polarization ensuring that unpolarized visible light will efficiently reach the protein monolayer also with backside illumination since we expect to have a random orientation of the membrane patches within the sample. The mid-IR transmittance decrease to 0.30–0.60 between 3 and 5 μm (3300–2000 cm^{-1}) due to absorption in SiO_2. In more detail the drop at around 3300 cm^{-1} corresponds to the O-H stretching mode of silanol groups (Si-OH) of the soda lime substrate. The transmittance vanishes for wavelengths greater than 5 μm as the substrate is completely opaque and it can be characterized only in reflectance mode.

2.2 Far-field polarization dependent IRRAS spectra

We have studied the polarization response of our nanorod platform down to the mid-IR range by means of IRRAS spectroscopy (see sketched in Fig. 2a). There are four possible configurations in which one can impinge with linearly polarized radiation on our sample, depicted in Figure 2c, two with TM (green and orange curves) and two with TE (blue and pink curves) polarization.

For each polarization, the data are collected rotating the sample by 90° in order to have: (1) TE polarization and E oriented parallel (TE-Long axis, blue curve) or perpendicular (TE-Short axis, pink curve) to main axis of the nanorods; (2) TM polarization and E whose in-plane component is oriented parallel (TM-Long axis, orange curve) or perpendicular (TM-Short axis, green curve) to the main axis of nanorods. Figure 2b reports a representative SEM image of the nanorod platform with the direction of E vector drawn when it is perpendicular or parallel to the main axis of nanorods for both TE and TM polarization, in the latter case considering the in-plane component of the E only.

In all curves the transverse (TO) and longitudinal optical (LO) phonons of SiO_2 are visible between 1000 and 1200 cm^{-1}. One might notice that LO phonons are not visible in normal incidence IR spectra for the transverse nature of electromagnetic waves, but become visible for grazing angle incidence [32]. For spectra taken with TM polarization we mostly see the phonons of the SiO_2 substrate, and no difference is found when rotating the samples, *i.e.*, by having the in-plane component of the E parallel or perpendicular to the nanorods. We ascribe this to the high incidence angle of 80° that leads to a very small in-plane component of the E impinging.

With TE polarization not only we find an overall higher reflectance but one can notice a strong modification of the phonon visibility on the relative direction of the E and the long axis of the nanorods: indeed, when the incident E is parallel to the main axis of nanorods, a reduction of the visibility of the LO phonon mode of SiO_2 is found and we interpret this as an indirect proof that a plasmonic resonance is sustained by our nanorods.

2.3 Near-field optical characterization of nanorod array platform

Since the main application, that can be foreseen for this kind of plasmonic devices, is to use them for enhanced

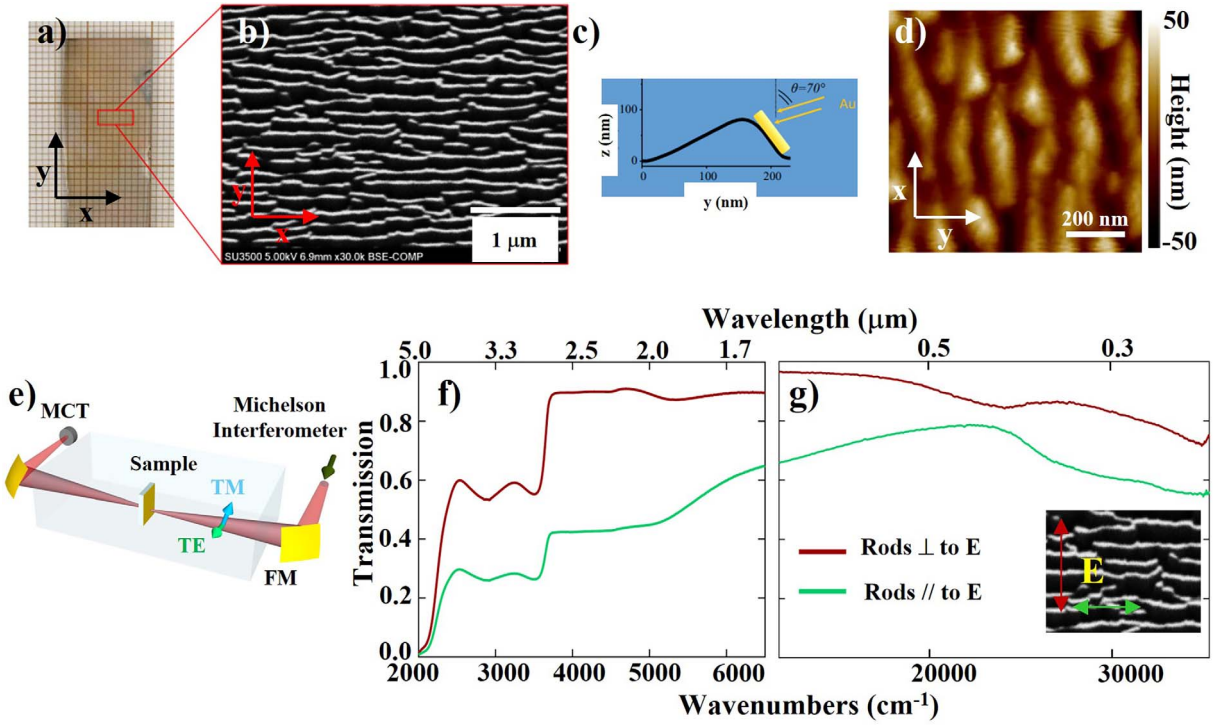

Fig. 1. (a) Visible image of the large-area nanorod platform showing the partial transparency of the sample. The sample is placed on a sheet of graph paper in order to highlight the spatial dimensions. (b) Representative SEM image. (c) Sketch of the ripple cross section for the nanorod platform. (d) AFM topography image of the nanorod platform. Note the disordered, although strongly anisotropic, arrangement of the gold nanorod array. (e) Sketch of the optical setup used to perform IR spectroscopy in transmission mode: the incoming IR radiation is focused by a parabolic mirror (FM) onto the sample. The radiation is linearly polarized by a wire-grid polarizer (the directions of E vector for both TE- and TM-polarized light are indicated by arrows in Figure). After the interaction with the sample, the IR radiation is focused onto an HgCdTe (MCT) photovoltaic detector. (f, g) Dichroic transmittance in the IR (f) and VIS (g) range for the two possible polarizations, *i.e.*, with E parallel or perpendicular to the main axis of nanorods.

spectroscopy, we performed near-field optical imaging to characterize the distribution of the hotspots and their dependence on the polarization of the impinging E. Therefore, we relied on photo-thermal induced resonance IR nanospectroscopy also called AFM-IR (see sketched in Fig. 3a) [33]. The IR intensity is acquired by monitoring the wavelength-dependent sample thermal expansion induced by the absorption of a mid-IR laser through the readout of the cantilever oscillation amplitude of an AFM. The AFM-IR signal can be modelled as:

$$\text{Photoexpansion signal}\,(x, y, \lambda) \propto \alpha(x, y, \lambda) \times V_{\text{exc}} \times I_{\text{laser}}$$

where $\alpha(x, y, \lambda)$ is the sample absorption coefficient, V_{exc} is the sample volume probed by IR radiation, I_{laser} is the IR radiation intensity [34, 35]. We have acquired the AFM-IR spectra of the nanorod platform with TE- and TM-polarized light impinging with an angle of 70° with respect to the sample surface normal. Figure 3b top, reports the AFM-IR spectra acquired positioning the AFM tip on top of a nanorod with TE polarization for both experimental configurations: when the main axis of nanorods is parallel to E (blue curve, TE-Long axis) and perpendicular to E (pink curve, TE-Short axis). The latter curve (TE-Short axis) shows two bands at 1080 and 1250 cm^{-1} related to the TO and LO phonons excitation. The blue curve (TE-Long axis) shows a suppression of the LO modes similarly to what seen in far-field because of the screening of free carriers excited along the rods. Figure 3b bottom, reports the AFM-IR spectra acquired with TM polarization when the main axis of nanorods is parallel to E (orange curve, TM-Long axis) and perpendicular to E (green curve, TM-Short axis). Also for TM polarization, the AFM-IR absorption spectra display the two bands at 1080 and 1200 cm^{-1} related to the TO and LO phonons excitation of SiO_2, mirroring the far-field IRRAS reflectance spectra (Fig. 2c).

AFM height maps and IR maps for TM and TE polarizations of a representative sample area of 3 × 3 μm^2 are reported in Figures 3c and 3d and Figures 3e and 3f, respectively. The IR maps are acquired by scanning the AFM tip on the sample area at fixed wavelength λ = 6.2 µm (1600 cm^{-1}). Figures 3g and 3h report the infusion maps of AFM height maps and IR maps for both polarizations in which the purple regions are the locations with higher IR absorption. For getting precise correlated maps, the drift is taken into consideration. We can notice that depending on the local configuration of the nanorods we get in the same sample region hotspots in slightly different regions, showing however that high IR intensity can be found in several spots, allowing us to average in a far-field sensing experiment over several of them, for both TE- and

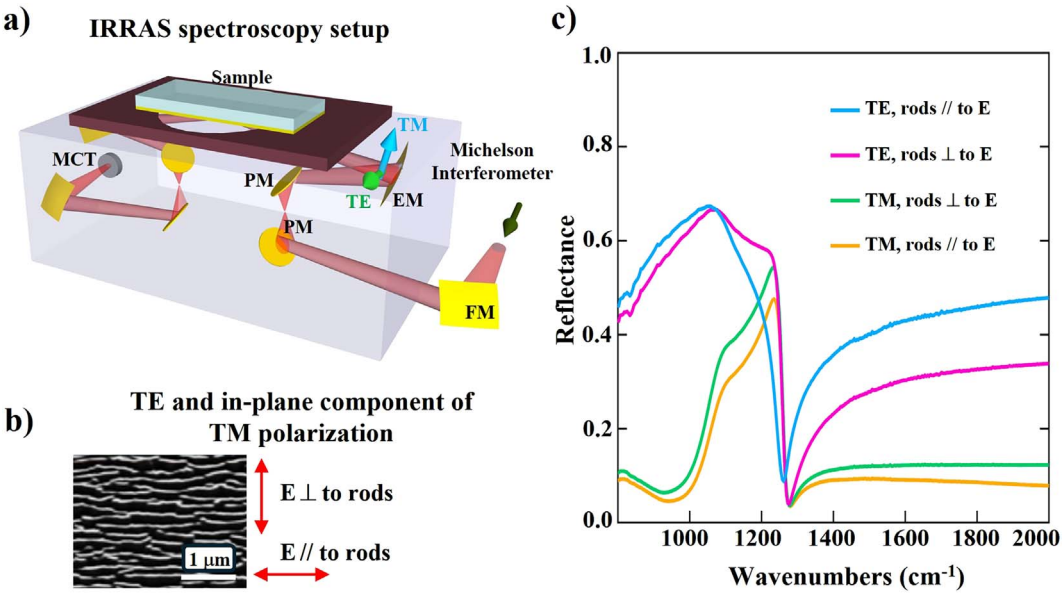

Fig. 2. (a) Sketch of the optical setup used to perform IRRAS spectroscopy: the incoming IR radiation, reflected by a parabolic mirror (FM) and two plane mirrors (PM), is focused by an elliptic mirror (EM) on the nanorod platform positioned in the upper part of the sample compartment. The radiation impinges with a grazing angle of 80° and it is linearly polarized by a wire-grid polarizer (the directions of E vector for both TE- and TM-polarized light are indicated by arrows in Figure). The outgoing IR radiation is focused finally onto an MCT photovoltaic detector through a specular mirror system. (b) Representative SEM image of the nanorod platform with the direction of E vector drawn when it is perpendicular or parallel to the main axis of nanorods, depending on the relative in-plane orientation of our sample and the E polarization. (c) IRRAS reflectance spectra of our sample when the main axis of nanorods is parallel to E using TE- (blue curve) and TM-polarized light (orange curve) and when the main axis of nanorods is perpendicular to E (pink curve and green curve for TE- and TM-polarized light, respectively).

TM-polarized light. Figure A1 in Appendix reports infusion maps acquired at other fixed wavelength with both polarizations and both relative orientations of E and the main axis of the nanorods.

2.4 Application to bacteriorhodopsin thin biolayers: SEIRA spectroscopy

To verify that our nanorod platform is suitable for SEIRA spectroscopy to detect very thin biolayers, we drop cast a suspension of cell membranes containing the light-sensitive transmembrane protein Bacteriorhodopsin (BR). The thickness of BR film is on average less than a hundred of nanometers and it is measured by AFM analysis. We acquired IRRAS reflectance spectra of BR film with both polarizations and in the two possible relative orientation between the main axis of nanorods and the direction of E, *i.e.*, parallel, or perpendicular (Fig. 4a). All IRRAS reflectance spectra are normalized for the IRRAS spectra acquired on the bare nanorod platform without BR proteins on top ($R_{\mathrm{IRRAS}} = I_{\mathrm{BR}}/I_{\mathrm{sub.bare}}$ with I_{BR} and $I_{\mathrm{sub.bare}}$ the spectrum of nanorods with and without BR on top, respectively) as reported by Greenler [36]. In case of a thin biolayer cast on a continuous metal surface, according to IRRAS spectroscopy theory, no reflection band related to protein should be visible in case of TE polarization. We find instead that our TE spectra (blue and pink curves in Fig. 4a) show the amide bands of proteins, the amide I band around 1660 cm^{-1} related to the C=O stretching mode and the amide II band around 1540 cm^{-1} due to the N-H bending mode of the peptide bonds [8]. When there is a plasmonic resonance excitation (TE-Long-axis, blue curve) the amide bands are less pronounced, while for TE-Short axis (pink curve) the features are stronger. We expect the nanorods to produce intense hotspots at their end for TE-Long axis. For TE-Short axis we can instead expect a smaller in-plane contribution of the E, but given their broad length distribution, an in-plane component of the field can be present, and since the volumes probed between parallel nanorods are several orders of magnitude larger than the small in-gap volume (see Figs. 3c and 3d), the overall signal IR signal averaged over a large area can be stronger.

We can suggest that given the morphological complexity of our nanorod platform and a non-negligible phase shift in the E close to the nanorod surface there will be a non-zero in-plane E intensity for TE polarization, for E parallel to both short axis and long axis.

For TM polarization (orange and green curves in Fig. 4a) we find that the most prominent feature is the amide I band, as expected since the C=O bond of the BR protein is aligned perpendicularly to the substrate/nanorod surface, while the amide II (the N-H bending mode is inversely aligned parallel to the substrate/nanorod surface) shows up as a weak dip in the reflectance spectra. This originates from two different factors: a thickness of about 100 nm on the biolayer film (only on a single protein monolayer the amide II band would become negligible) and a contribution of the nanorods that provide weak in-plane E [37, 38].

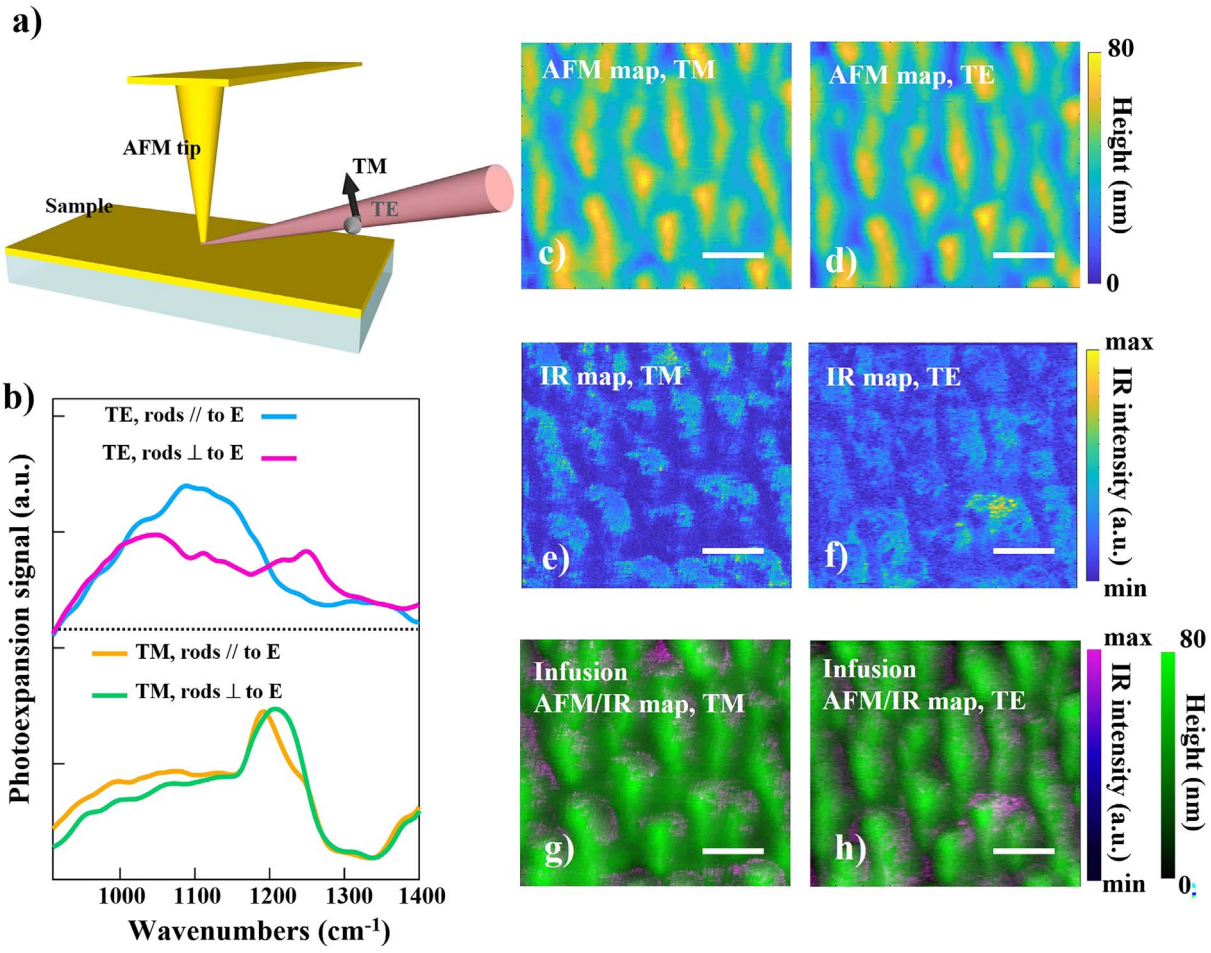

Fig. 3. (a) Sketch of AFM-IR setup with an oblique incidence of IR radiation of 70° with respect to the sample surface normal. (b) Top, AFM-IR absorption spectra in TE polarization with E parallel (blue curve, TE-Long axis) and perpendicular (pink curve, TE-Short axis) to the main axis of the nanorods. Bottom, same of top for TM polarization: orange curve and green curve for TM-Long axis and TM-Short axis, respectively. (c, d) AFM height maps for TM (c) and TE (d) polarizations and (e, f) IR maps at 1600 cm^{-1} ($\lambda = 6.2$ μm) for TM (short-axis) (e) and TE (long-axis) (f) polarizations. In order to acquire these maps, we have covered the nanorods with a thin polymer layer. (g, h) Infusion maps of AFM height maps and IR maps for TM (g) and TE (h) polarizations. It is possible to identify regions with higher IR intensity for both polarizations of the impinging radiation. For all maps the scale bar is 200 nm.

2.5 Application to bacteriorhodopsin thin biolayers: difference IRRAS spectroscopy

BR is a transmembrane protein sensitive to green visible light. Following light absorption, BR can move protons across the cell membrane thanks to a very fast retinal photo-isomerization and to a slower cyclic sequence of conformational changes of the protein backbone (also referred to as a "photocycle") [24, 25]. To isolate the extremely small ($\leq 10^{-3}$) light-induced changes in IR absorption, difference spectroscopy schemes (visible light ON minus visible light OFF) are employed typically on re-hydrated thick films or on liquid suspensions containing large numbers of proteins due to the poor sensitivity of IR spectroscopy [9, 39]. Here we were able to monitor the polarization-resolved light-induced conformational changes of a reduced number of BR proteins forming a film of thickness of less than a hundred of nanometers, by using the combination of our plasmonic platform with the difference IRRAS spectroscopy. To start the BR photocycle, the sample is illuminated with a LED emitting at 565 nm from the backside of the platform exploiting its transparency. In Figure 4c, the IRRAS difference spectra are reported, the blue curve in TE polarization and the orange curve in TM polarization with the E component parallel to the main axis of nanorods, *i.e.*, the two configurations in which a plasmonic behavior of our platform is expected. The grey curve in Figure 4c is the difference spectrum acquired on a 2-μm thick film of BR proteins deposited on a CaF_2 window in transmission mode used as a benchmark. In this case we expect to have a more or less isotropic orientation of the BR helices. In the IRRAS difference spectra, positive and negative peaks related to light-induced conformational changes of BR proteins are clearly identified. If comparing the difference spectra collected in TE and TM polarizations one can note several differences. In the spectral region of the amide I

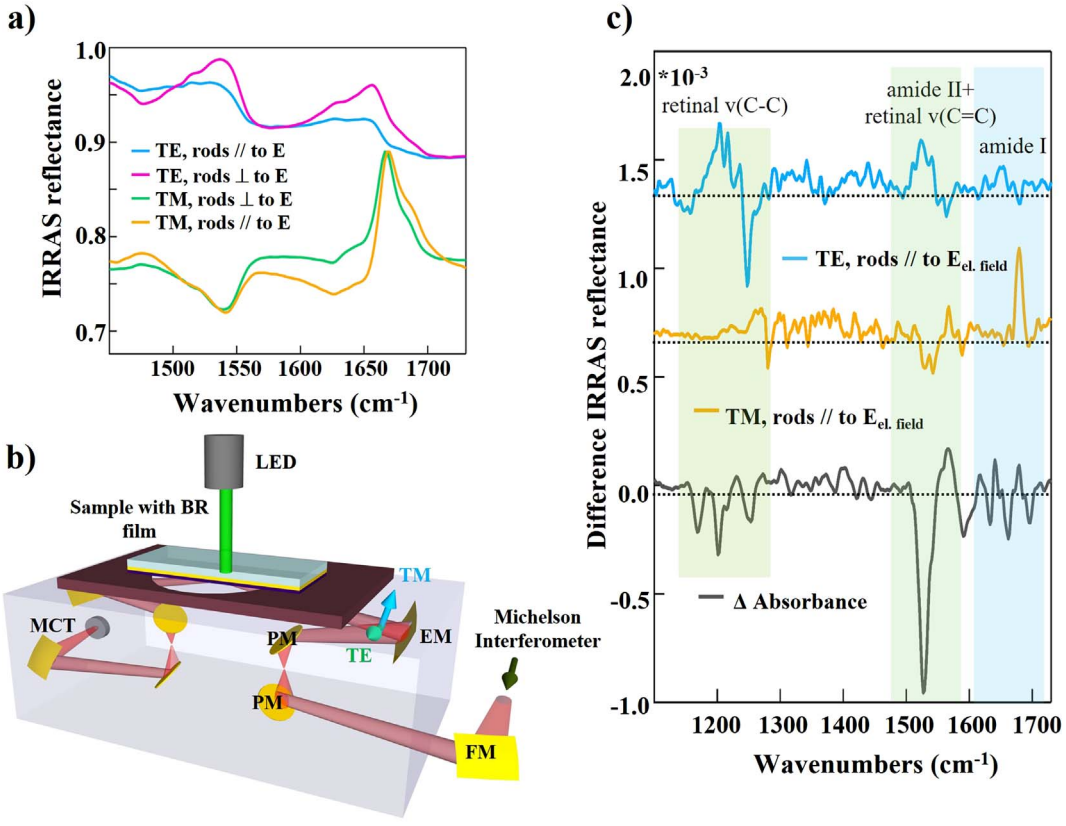

Fig. 4. (a) IRRAS reflectance spectra in the amide bands region of the nanorod platform with BR film deposited on top for all four possible configurations of nanorod orientation and light polarization. (b) Sketch of the experimental IRRAS setup to perform difference IRRAS spectroscopy of BR proteins. The green light emitted by a LED at 565 nm is sent to the backside of the platform exploiting its semi-transparency and it is used to start the BR photocyle. (c) IRRAS difference spectra of the nanorod platform with BR film using TE- (blue curve) and TM-polarized light (orange curve). For both curves the main axis of nanorods is parallel to E. The FTIR difference spectrum acquired on a 2-μm thick film of BR proteins deposited on a CaF_2 window in transmission mode is reported as grey curve.

band (1620–1680 cm^{-1}, blue region in Fig. 4c) it is clearly visible one intense feature for TM polarization that we explain due to the co-alignment of the C=O bonds of the protein backbone and the component of the E orthogonal to the substrate/nanorod surface that we expect to be strongest in this configuration. On the other hand, for TE polarization the peaks are really weak, as one can expect. One can note that instead in the spectral region that highlights modifications of the retinal (green regions in Fig. 4c) some peaks are completely different, and that some others are instead have opposing sign for the two polarizations, suggesting that in this case we can monitoring an overall rotation of the associated dipole moments.

3 Conclusion

We discuss the possibility to study polarization-resolved light-induced conformational changes of BR proteins drop cast on gold nanorods deposited on SiO_2. We exploit the transparency of the nanorod platform to perform difference IRRAS spectroscopy (visible light ON minus visible light OFF) with simultaneous visible light illumination from the backside of the platform. In our experiment we combine IRRAS with self-organized plasmonic nanorods in order to be able to probe with high sensitivity the modifications of the vibrational peaks over the entire fingerprint region. We show that it is possible to identify differences in the IRRAS difference spectra that imply we are monitoring over a broadband frequency range not only the chemical bonds with the dipole moment aligned orthogonally to our substrate/nanorod surface. This work is a first step into the polarization-resolved broadband sensing and conformational study of transmembrane proteins.

4 Materials and methods

4.1 Sample fabrication and morphology

Large area self-organized nanopatterns are obtained over large-area (cm^2) by defocused ion beam sputtering of low-cost glass substrates (soda-lime). Glass substrates are irradiated by means of a *Tectra GmhB* ion gun operating in Ar atmosphere at the pressure of 4.0×10^{-4} mbar and generating an ion beam of 800 eV energy. The substrate

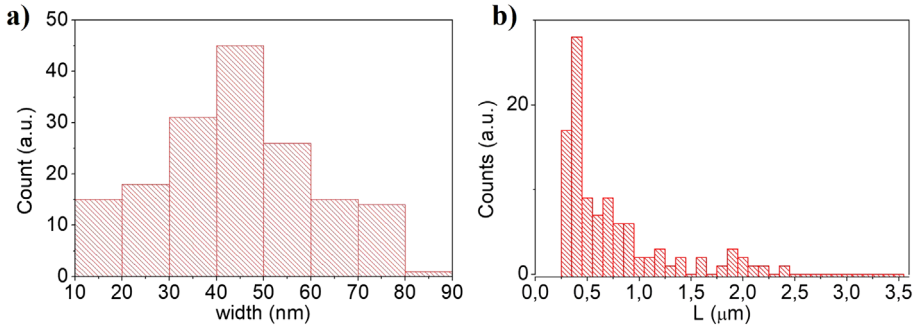

Fig. 5. Histograms of nanorods width (a) and length (b) measured by the statistical analysis of SEM images of the sample.

is irradiated at 30° incidence angle with respect to the glass surface normal, as described in detail in reference [29] with an ion fluence of 1.4×10^{19} ions/cm^2. To promote pattern formation under an ion induced wrinkling instability the sample is heated up to about 680 K temperature during the sputtering process.

This nanopatterned templates effectively promote confinement of anisotropic arrays of gold nanorods by glancing angle thermal evaporation perpendicular to the faceted glass nanoridges. Gold nanorods are confined on the short ripples facets (tilted at $\theta_{\text{facets}} = 50°$) by evaporation at θ_{Au} beam $= 70°$ with respect to the mean plane normal direction.

The local thickness of the gold stripes h is controlled by means of a calibrated quartz microbalance measuring the gold thickness deposited on a flat substrate (h_0). By basic trigonometric arguments the local thickness on the facets can be calculated $h = h_0 \times \cos(|\theta_{\text{Au beam}} - \theta_{\text{facet}}|)$. The distribution of the nanorods width, w, and length, L, is measured by the statistical analysis of SEM images of the sample. In Figure 5, the histograms of nanorods width (Fig. 5a) and length (Fig. 5b) are shown. The mean width reads about 45 nm with a relatively narrow distribution of size from 10 nm up to 70 nm, imposed by the template nanopattern. Conversely the nanorods length distribution is broad, extending from 250 nm up to 2 μm, with few counts up to 3.5 μm.

4.2 Cell membrane sample preparation

Patches of cell membranes containing BR were isolated as reported in reference [40] and stored in buffer solution (20 mM Bis-Tris propane, 100 mM NaCl, 1 mM MgCl2) at −80 °C. The thickness of an individual patch of cell membrane is 5 nm and the protein:lipid ratio is 75:25. For the IRRAS characterization, 6 μL of the suspension containing cell membranes were drop cast onto the nanorod platform for 3 min, then rinsed with 50 μL Milli-Q water and let dry in air.

4.3 IR spectroscopy

IR measurements in Figure 1f were performed in transmission mode with a Bruker VERTEX 80v spectrometer (*Bruker Optic GmbH*, Ettlingen, Germany) using an internal IR source and a MCT detector in vacuum condition. Spectra were recorded with a spectral resolution of 2 cm^{-1} and 512 interferometer scans using either perpendicular or parallel polarized light.

4.4 VIS spectroscopy

Normal incidence extinction spectra were acquired in the 300–1100 nm spectral range by coupling a compensated halogen-deuterium lamp (DH-2000-BAL, *Mikropak*) to a Vis-NIR spectrometer (HR4000, *Oceans Optics*) via fiber optics. The spot size is macroscopic with a diameter of about 2 mm. For linearly polarized measurements, a *Thorlabs Glen-Thompson* Polarizer was used, with a flat, bare glass serving as the reference. Normal incidence extinction spectra were also acquired in the Near Infrared (1000–2000 nm wavelength) by fiber coupling the same optical setup to a solid state Infrared spectrometer (*Arcoptix*).

4.5 IRRAS spectroscopy

IRRAS spectroscopy spectra were recorded with a Bruker VERTEX 80v spectrometer (*Bruker Optic GmbH*, Ettlingen, Germany) using a mirror system sketched in Figure 2a to focus polarized IR light onto the sample at a grazing angle of 80°. For the nanorod platform characterization (Fig. 2c), spectra were recorded with a spectral resolution of 2 cm^{-1} and 512 interferometer scans, using an aperture with a diameter of 1.5 mm. The measurements of the nanorod platform were referenced to the measurements of a reference gold substrate. For the nanorod platform with BR proteins on top characterization (Fig. 4a), spectra were recorded with a spectral resolution of 2 cm^{-1} and 1024 interferometer scans, using an aperture with a diameter of 1.5 mm. The measurements were referenced to the measurements of the nanorod platform without BR proteins on top.

4.6 IRRAS difference spectroscopy

IRRAS difference spectroscopy was performed by implementing a system of visible illumination to control BR photocycle. Visible light was provided by a LED (Thorlabs M565L3, center wavelength at 565 nm) and the power sent to the sample was around 10 mW/cm^2. The reflectance intensity was collected both in dark condition (R_{dark}) and under visible illumination (R_{green}) by averaging 256 interferometer scans at 2 cm^{-1} spectral resolution.

The difference IRRAS spectra in Figure 4c were calculated as: $-\log(R_{green}/R_{dark})$ by averaging over 100 illumination cycles.

4.7 AFM-IR imaging and nanospectroscopy

The AFM-IR imaging and nanospectroscopy were performed using a NanoIR2 system by Anasys Instrument relied on the photothermal expansion effect. The IR radiation impinges on the sample from the side at an angle of 70° and it is provided by an external-cavity broadly tunable quantum cascade laser (QCL) (MIRCATxB, by *Daylight Solutions*) with a spectral range 900–1800 cm^{-1}. The duration time of light pulses is 260 ns long and the laser repetition rate is chosen as to be in resonance with the second mechanical bending mode frequency of the cantilever (≈200 kHz). Commercial gold-coated AFM probes provided by Anasys/Bruker with free resonant frequency of 13 kHz and spring constant between 0.07 and 0.4 N/m were employed. The curvature radius of the probe tip apex is around 25 nm. AFM-IR spectra in Figure 3b were acquired with 4 cm^{-1} steps, with ≈0.3 s per step subdivided in tuning time and integration time. A smoothing spline algorithm has been applied to obtain the final AFM-IR spectra shown in Figure 3b. The AFM and AFM-IR images in Figures 3c and 3h were taken at 0.3 Hz with 100 × 100 points.

Funding

All the authors acknowledge support from the PRIN 2022 PNRR program, grant No. P2022JWKAC. M.C. Giordano acknowledges support from "Progetto Curiosity driven 2021" funded by *European Union – Next Generation EU.*

Conflicts of Interest

The authors declare no conflict of interest.

Data availability statement

Data will be made available from the corresponding author upon reasonable request.

Author contribution statement

FBM, MO, LB, and MCG: conceptualization, methodology, and design of the experiments; RP, SS, FS, GF, MET, VG, LB and MCG: investigation, RP, SS, FS, FB, MET, MO, and LB: analysis, and interpretation of the results; RP, FB, and LB: writing – original draft; all authors: writing – review and editing.

References

1 Baker M.J., Trevisan J., Bassan P., Bhargava R., Butler H.J., Dorling K.M., Fielden P.R., Fogarty S.W., Fullwood N.J., Heys K.A., Hughes C., Lasch P., Martin-Hirsch P.L., Obinaju B., Sockalingum G.D., Sulé-Suso J., Strong R.J., Walsh M.J., Wood B.R., Gardner P., Martin F.L. (2014) Using Fourier transform IR spectroscopy to analyze biological materials, *Nat. Protoc.* **9**, 1771–1791.

2 Brown L.V., Yang X., Zhao K., Zheng B.Y., Nordlander P., Halas N.J. (2015) Fan-shaped gold nanoantennas above reflective substrates for surface-enhanced infrared absorption (SEIRA), *Nano Lett.* **15**, 1272–1280.

3 Dong L., Yang X., Zhang C., Cerjan B., Zhou L., Tseng M.L., Zhang Y., Alabastri A., Nordlander P., Halas N.J. (2017) Nanogapped Au Antennas for ultrasensitive surface-enhanced infrared absorption spectroscopy, *Nano Lett.* **17**, 5768–5774.

4 Rodrigo D., Limaj O., Janner D., Etezadi D., De Abajo F.J.G., Pruneri V., Altug H. (2015) Mid-infrared plasmonic biosensing with graphene, *Science* **349**, 165–168.

5 Ataka K., Tilman K., Joachim Heberle H. (2010) Thinner, smaller, faster: IR techniques to probe the functionality of biological and biomimetic systems, *Angew. Chem. Int. Ed.* **49**, 32, 5416–5424.

6 López-Lorente Á.I., Mizaikoff B. (2016) Mid-infrared spectroscopy for protein analysis: potential and challenges, *Anal. Bioanal. Chem.* **408**, 2875–2889.

7 Ernst O.P., Lodowski D.T., Elstner M., Hegemann P., Brown L.S., Kandori H. (2014) Microbial and animal rhodopsins: structures, functions, and molecular mechanisms, *Chem. Rev.* **114**, 1, 126–163.

8 Barth A. (2007) Infrared spectroscopy of proteins, *Biochim. Biophys. Acta-Bioenergetics* **1767**, 9, 1073–1101.

9 Lorenz-Fonfria V.A. (2020) Infrared difference spectroscopy of proteins: from bands to bonds, *Chem. Rev.* **120**, 7, 3466–3576.

10 Blume A., Kerth A. (2013) Peptide and protein binding to lipid monolayers studied by FT-IRRA spectroscopy, *Biochim. Biophys. Acta-Biomembranes* **1828**, 10, 2294–305.

11 Enders D., Pucci A. (2006) Surface Enhanced Infrared Absorption of Octadecanethiol on Wet-Chemically prepared Au Nanoparticle Films, *Appl. Phys. Lett.* **88**, 184104.

12 Hoffmann F.M. (1983) Infrared reflection-absorption spectroscopy of adsorbed molecules, *Surf. Sci. Rep.* **3**, 2, 107–192.

13 Occhicone A., Pea M., Polito R., Giliberti V., Sinibaldi A., Mattioli F., Cibella S., Notargiacomo A., Nucara A., Biagioni P., Michelotti F., Ortolani M., Baldassarre L. (2020) Spectral Characterization of mid-infrared Bloch surface waves excited on a truncated 1D photonic crystal, *ACS Photonics* **8**, 1, 350–359.

14 Biagioni P., Huang J.S., Hecht B. (2012) Nanoantennas for visible and infrared radiation, *Rep. Prog. Phys.* **75**, 2, 024402.

15 Neubrech F., Huck C., Weber K., Pucci A., Giessen H. (2017) Surface-enhanced infrared spectroscopy using resonant nanoantennas, *Chem. Rev.* **117**, 7, 5110–5145.

16 Adato R., Altug H. (2013) In-situ ultra-sensitive infrared absorption spectroscopy of biomolecule interactions in real time with plasmonic nanoantennas, *Nat. Commun.* **4**, 1, 2154.

17 Adato R., Yanik A.A., Amsden J.J., Kaplan D.L., Omenetto F.G., Hong M.K., Erramilli S., Altug H. (2009) Ultra-sensitive vibrational spectroscopy of protein monnolayers with plasmonic nanoantenna arrays, *Proc. Natl. Acad. Sci.* **106**, 46, 19227–19232.

18 Temperini M.E., Di Giacinto F., Romanò S., Di Santo R., Augello A., Polito R., Baldassarre L., Giliberti V., Papi M., Basile U., Niccolini B., Krasnowska E.K., Serafno A., De Spirito M., Di Gaspare A., Ortolani M., Ciasca G. (2022) Antenna-enhanced mid-infrared detection of Extracellular Vesicles derived from human cancer cell cultures, *J. Nanobiotechnol.* **20**, 1, 530.

19 Neubrech F., Pucci A., Cornelius T.W., Karim S., García-Etxarri A., Aizpurua J. (2008) Resonant plasmonic and vibrational coupling in a tailored nanoantenna for infrared detection, *Phys. Rev. Lett.* **101**, 15, 157403.

20 Adato R., Serap A., Hatice A. (2015) Engineering mid-infrared nanoantennas for surface enhanced infrared absorption spectroscopy, *Mater. Today* **18**, 8, 436–446.

21 Rodrigo D., Tittl A., Ait-Bouziad N., John-Herpin A., Limaj O., Kelly C., Yoo D., Wittenberg N.J., Oh S.H., Lashuel H.A., Altug H. (2018) Resolving molecule-specific information in dynamic lipid membrane processes with multi-resonant infrared metasurfaces, *Nat. Commun.* **9**, 1, 2160.

22 Aouani H., Sipova H., Rahmani M., Navarro-Cia M., Hegnerova K., Homola J., Hong M., Maier S.A. (2013) Ultrasensitive broadband probing of molecular vibrational modes with multifrequency optical antennas, *ACS Nano* **7**, 1, 669–675.

23 D'Andrea C., Bochterle J., Toma A., Huck C., Neubrech F., Messina E., Fazio B., Marago O.M., Di Fabrizio E., Lamy de La Chapelle M., Gucciardi P.G., Pucci A. (2013) Optical Nanoantennas for Multiband Surface-Enhanced Infrared and Raman Spectroscopy, *ACS Nano* **7**, 4, 3522–3531.

24 Haupts U., Tittor J., Oesterhelt D. (1999) Closing in on bacteriorhodopsin: progress in understanding the molecule, *Annu. Rev. Biophys. Biomol. Struct.* **28**, 367–399.

25 Lanyi J.K. (2006) Proton transfers in the bacteriorhodopsin photocycle, *Biochim. Biophys. Acta-Bioenergetics* **1757**, 8, 1012–1018.

26 Giordano M.C., Longhi S., Barelli M., Mazzanti A., Buatier de Mongeot F., Della Valle G. (2018) Plasmon hybridization engineering in self-organized anisotropic metasurfaces, *Nano Research* **11**, 3943–3956.

27 Barelli M., Giordano M.C., Gucciardi P.G., Buatier de Mongeot F. (2020) Self-organized nanogratings for large-area surface plasmon polariton excitation and surface-enhanced Raman spectroscopy sensing, *ACS Appl. Nano Mater.* **3**, 9, 8784–8793.

28 Giordano M.C., Tzschoppe M., Barelli M., Vogt J., Huck C., Canepa F., Pucci A., Buatier de Mongeot F. (2020) Self-organized nanorod arrays for large-area surface-enhanced infrared absorption, *ACS Appl. Mater. Interfaces* **12**, 9, 11155–11162.

29 Giordano M.C., Buatier de Mongeot F. (2018) Anisotropic nanoscale wrinkling in solid-state substrates, *Adv. Mater.* **30**, 30, 1801840.

30 Giordano M.C., di Sacco F., Barelli M., Portale G., Buatier de Mongeot F. (2021) Self-organized tailoring of faceted glass nanowrinkles for organic nanoelectronics, *ACS Appl. Nano Mater.* **4**, 1940–1950.

31 Barelli M., Mazzanti A., Giordano M.C., Della Valle G., Buatier de Mongeot F. (2020) Color routing via cross-polarized detuned plasmonic nanoantennas in large-area metasurfaces, *Nano Lett.* **20**, 6, 4121–4128.

32 Almeida Rui M. (1992) Detection of LO modes in glass by infrared reflection spectroscopy at oblique incidence, *Phys. Rev. B* **45**, 1, 161–170.

33 Lu F., Jin M., Belkin M.A. (2014) Tip-enhanced infrared nanospectroscopy via molecular expansion force detection, *Nat. Photonics* **8**, 4, 307–312.

34 Lu F., Belkin M.A. (2011) Infrared absorption nano-spectroscopy using sample photoexpansion induced by tunable quantum cascade lasers, *Opt. Express* **19**, 21, 19942–19947.

35 Giliberti V., Polito R., Ritter E., Broser M., Hegemann P., Puskar L., Schade U., Zanetti-Polzi L., Daidone I., Corni S., Rusconi F., Biagioni P., Baldassarre L., Ortolani M. (2019) Tip-enhanced infrared difference-nanospectroscopy of the proton pump activity of bacteriorhodopsin in single purple membrane patches, *Nano Lett.* **19**, 5, 3104–3114.

36 Greenler R.G. (1966) Infrared study of adsorbed molecules on metal surfaces by reflection techniques, *J. Chem. Phys.* **44**, 1, 310–315.

37 Giliberti V., Badioli M., Nucara A., Calvani P., Ritter E., Puskar L., Aziz E.F., Hegemann P., Schade U., Ortolani M., Baldassarre L. (2017) Heterogeneity of the transmembrane protein conformation in purple membranes identified by infrared nanospectroscopy, *Small* **13**, 44, 1701181.

38 Polito R., Temperini M.E., Ritter E., Puskar L., Schade U., Broser M., Hegemann P., Baldassarre L., Ortolani M., Giliberti V. (2021) Conformational changes of a membrane protein determined by infrared difference spectroscopy beyond the diffraction limit, *Phys. Rev. Appl.* **16**, 014048.

39 Ritter E., Puskar L., Bartl F.J., Aziz E.F., Hegemann P., Schade U. (2015) Time-resolved infrared spectroscopic techniques as applied to channelrhodopsin, *Front. Mol. Biosci.* **2**, 38.

40 Oesterhelt D., Stoeckenius W. (1974) Isolation of the cell membrane of Halobacterium halobium and its fractionation into red and purple membrane, *Methods Enzymol* **31**, 667–678.

Appendix A

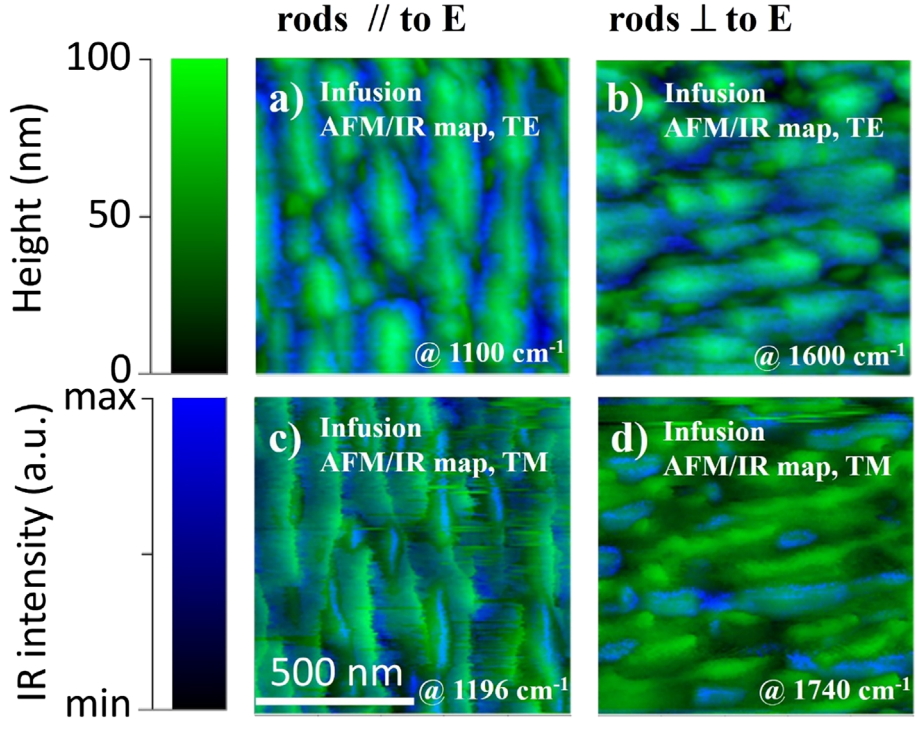

Fig. A1. (a, b) Infusion maps of AFM height maps (green scale bar) and IR maps (blue scale bar) for TE polarization with E parallel (a) and perpendicular (b) to the main axis of the nanorods. IR maps are acquired at 1100 cm^{-1} and 1600 cm^{-1} for (a) and (b), respectively. (c, d) Infusion maps of AFM height maps and IR maps for TM polarization with E parallel (c) and perpendicular (d) to the main axis of the nanorods. IR maps are acquired at 1196 cm^{-1} and 1740 cm^{-1} for (a) and (b), respectively. In all infusion maps, regardless of light polarization and relative orientations between E and the main axis of the nanorods, it is possible to identify an overall distribution of blue regions with higher IR intensity.